Computing of 93Nb NMR Parameters of Solid-State Niobates. The Geometry Matters

Ibtissam Saouli, Sylvain Landron, Berislav Peric, Ahmed Boutarfaia, Cassandre Kouvatas, Laurent Le Pollès, Jérôme Cuny, Régis Gautier

COMPUTING ^{93}NB NMR PARAMETERS OF SOLID-STATE NIOBATES. THE GEOMETRY MATTERS.

Ibtissam Saouli,[ab] Sylvain Landron,[a] Berislav Peric,[ac] Ahmed Boutarfaia,[b] Cassandre Kouvatas,[a] Laurent Le Pollès,[a] Jérôme Cuny,[d] and Régis Gautier[a]

[a] *Univ Rennes, Ecole Nationale Supérieure de Chimie de Rennes, CNRS, ISCR – UMR 6226, F-35000, Rennes, France*

[b] *Faculté des Sciences et de la Technologie et Sciences de la Matière, Université Merbah Kasdi-Ouargla, Ouargla, Algeria*

[c] *Laboratory for Solid-State and Complex Compounds Chemistry, Division of Materials Chemistry, Ruđer Bošković Institute, Bijenička cesta 54, 10000-HR, Zagreb, Croatia*

[d] *Laboratoire de Chimie et Physique Quantiques, IRSAMC, Université Paul Sabatier, 118 Route de Narbonne, 31062 Toulouse Cedex 4, France*

E-mail: rgautier@ensc-rennes.fr

ABSTRACT

This work aims at studying the influence of structural parameters on the computations of ^{93}Nb quadrupolar interaction and chemical shift parameters in various niobates using first-principles approaches. We demonstrate that some of the computed NMR parameters, especially the isotropic chemical shift and the quadrupolar coupling constant, may differ either the X-ray crystal structure or a relaxed structure are used for the calculation of the spectroscopic properties.

Keywords: NMR, DFT, Niobates, Chemical shift, Quadrupolar interaction

INTRODUCTION

Nuclear Magnetic Resonance (NMR) applied to solid is a powerful and increasingly important technique for the characterization of a wide range of structural materials. The transition metal nuclei often exhibit very large chemical shift ranges that may extend to more than thousand parts per million (ppm). Therefore, this parameter becomes extremely sensitive to small changes in the environment of the probed nucleus. The nuclear quadrupole moment is a fundamental character associated with the nucleus that is related to the non-pure spherical distribution of the charge. The quadrupole moment measuring method consists in studying the electrical hyperfine interaction energy between the quadrupole moment and the gradient of the electric field due to atomic electrons. Therefore, this parameter is also very sensitive to the environment of the probed nucleus. In particular, the effects of covalency in the NMR parameters may be quite important [1,2,3,4,5,6].

The combination of several interactions often makes complex solid-state NMR spectra and it is frequently difficult to extract all the information from these measurements. First-principles calculations are often used to complement experimental investigations. Density functional theory (DFT) is currently one of the most used methods in quantum calculations of the electronic structure of molecules and solids. More than thirty years ago, Blaha et al. developed a method for calculating electric field gradients (EFG) in solids using the linearized augmented planar wave (LAPW) approach [7]. In 1994, P. E. Blöchl developed a new approach called the projector augmented wave (PAW) method, which combines the versatility of the LAPW method with the formal simplicity of the traditional pseudopotential plane-wave approach [8]. This method allows the use of ultra-flexible pseudopotentials which are one of the crucial factors for saving CPU time. In 2001, C. Pickard and F. Mauri developed a method for calculating chemical shifts under periodic boundary conditions and the pseudopotential (PP) approximation [9]. This method has been used successfully to calculate NMR shielding in various types of transition metal compounds [10,11,12]. Laskowski and Blaha developed another formalism to compute nuclear shielding tensors within the LAPW and APW+lo frameworks [13,14] (APW+lo approach uses local orbitals for an improved convergence according to the number of PWs). Although recent, the few applications of this formalism have demonstrated a result quality almost equivalent to that of GIPAW for various nuclei [13,14,15].

^{93}Nb is a 9/2 spin nucleus with 100% natural abundance and a relatively large gyromagnetic ratio. It is thus a relatively sensitive nucleus (equal to 0.48). However, it suffers from a large nuclear quadrupole moment (Q =32 x10^{-30} m^2) and in the solid state, ^{93}Nb NMR spectra are dominated by

the second-order quadrupolar interaction. Thus, the resonance of the central transition (–1/2↔1/2) may be considerably broad. J. V. Hanna et al. studied several inorganic niobates using solid-state NMR [16]. They showed that both ^{93}Nb quadrupolar and chemical shift parameters are sensitive to structural details. They also computed NMR parameters using DFT periodic calculations. Later, E. Papulovskiy et al. completed these experimental and theoretical results for additional inorganic niobates [17]. Except for some structures, both computational investigations were carried out using X-ray crystallographic structures. Since some of us demonstrated that geometry optimizations of the crystal structures is a pre-requisite for accurate computed NMR parameters [18,19], we investigated the effect of geometry optimization on the computed ^{93}Nb NMR parameters of twelve niobates.

CONVENTIONS AND METHODS

Calculations give access to the shielding tensor expressed in the crystal frame. The three chemical shielding parameters, σ_{iso}, σ_{aniso}, and η_σ, are calculated from the eigenvalues (σ_{xx}, σ_{yy}, σ_{zz}) using the following equations:

$$\sigma_{iso} = \frac{(\sigma_{xx} + \sigma_{yy} + \sigma_{zz})}{3}$$

$$\sigma_{aniso} = (\sigma_{xx} - \sigma_{zz}) \text{ , with } \sigma_{xx} \geq \sigma_{yy} \geq \sigma_{zz}$$

$$\eta_\sigma = (\sigma_{yy} - \sigma_{xx})/(\sigma_{zz} - \sigma_{iso})$$

δ_{iso} is calculated from the isotropic shielding using the relation defined by E. Papulovskiy et al. in Ref. 17:

$$\delta_{iso} = 0.9774(-578.09 - \sigma_{iso})$$

The EFG tensor is traceless, that is, its eigenvalues (V_{xx}, V_{yy}, V_{zz}) obey $V_{xx} + V_{yy} + V_{zz} = 0$. We used the following conventions for the quadrupolar coupling constant C_Q and the asymmetric parameter η_Q:

$$C_Q = \frac{eQV_{zz}}{h}$$

$$\eta_Q = \frac{(V_{yy} - V_{xx})}{V_{zz}}$$

with $|V_{zz}| \geq |V_{yy}| \geq |V_{xx}|$

^{93}Nb NMR parameters were computed for both X-ray and relaxed crystal structures of eleven compounds. Two of these compounds exhibit four-coordinated NbO_4 sites ($LaNbO_4$ [20], $YNbO_4$

[21]) whereas the nine others exhibit six-coordinated NbO_6 sites ($MgNb_2O_6$ [22], $CaNb_2O_6$ [23], $SnNb_2O_6$ [24], $BiNbO_4$ [25], La_3NbO_7 [26], $Mg_4Nb_2O_9$ [27], $CsBiNb_2O_7$ [28], $Cd_2Nb_2O_7$, (tetragonal [29] and cubic [30] structures), and $Sn_2Nb_2O_7$ [31]. Full geometry optimizations (cell parameters and atomic positions) were performed with the CASTEP 4.3 code [32] using the PBE functional [33]. The convergence parameters were set equal to 2×10^{-5} eV for d*E*/ion (energy convergence parameter per ion), 20 meV for $|F|_{max}$ (force convergence parameter), 10^{-3} for $|dr|_{max}$ (displacement convergence parameter), and 10^{-1} GPa for S_{max} (stress convergence parameter). Optimizations were performed using initial symmetry constraints automatically determined by CASTEP 4.3. All calculations were checked for convergence with respect to the kinetic energy cutoff of the plane waves basis set (up to 800 eV) and the k-points grid used for integration over the Brillouin zone (BZ).

PAW [8] and GIPAW [9] calculations were carried out with the CASTEP 4.3 code [32] using the same GGA functional [33]. A set of convergence test calculations with energy cut-off values ranging from 500 to 900 eV were performed with steps of about 200 eV. All calculations were proven to converge in EFG and CS values with a cut-off energy of 700 eV. Increasing the cut-off energy to 800 eV resulted in maximum variations of 0.01 MHz, 0.01, 1.00 ppm, 0.10 ppm and 0.01 for C_Q, η_Q, σ_{iso}, σ_{aniso} and η_σ, respectively. Different Monkhorst–Pack k-point grids for each compound were tested until convergence of the computed NMR parameters [34]. All USPP were generated using the OTF_ultra-soft PP generator included in CASTEP 4.3 [32]. Relativistic effects were taken into account for all elements by using the scalar relativistic PP.

APW + lo calculations were carried out using the WIEN2k code [35,36] in the PBE GGA [33] for the following compounds: $BiNbO_4$, La_3NbO_7, $Mg_4Nb_2O_9$, and $Sn_2Nb_2O_7$. X-ray and optimized crystal structures were both used to compute quadrupolar interaction and chemical shift NMR parameters. The optimized structures were relaxed using the CASTEP code. For all compounds, sphere sizes were determined automatically. An $R_{min}K_{max}$ value of 7 was used. Convergence of calculations was checked for each crystallographic structure with an $R_{min}K_{max}$ value of 8. All calculations were also converged towards the number of k-points used for the BZ integration.

RESULTS

The parameters computed for both X-ray and optimized crystal structures are reported in Table 1. The results will be discussed in the three following sections: Nb-O distances, quadrupolar interaction and chemical shift parameters.

TABLE 1. ^{93}Nb δ_{iso} (ppm) σ_{aniso} (ppm), η_σ, C_Q (MHz), η_Q, averaged and standard deviation of Nb-O distances (Å) computed using the CASTEP code from X-ray (roman) and optimized (italic) structures. ^{93}Nb NMR parameters computed using the WIEN2k code are given in parentheses.

	δ_{iso} *(ppm)*	σ_{aniso} *(ppm)*	η_σ	C_Q *(MHz)*	η_Q	Nb-O aver. (Å)	Nb-O std. dev. (Å)
$LaNbO_4$	911 *799*	430 *134*	0.73 *0.62*	123 *54*	0.22 *0.31*	1.851 *1.870*	0.066 *0.003*
$YNbO_4$	839 *905*	250 *249*	0.40 *0.52*	72 *76*	0.31 *0.41*	1.894 *1.890*	0.057 *0.033*
$MgNb_2O_6$	1000 *952*	493 *495*	0.28 *0.28*	50 *58*	0.27 *0.32*	2.015 *2.034*	0.147 *0.168*
$CaNb_2O_6$	1033 *913*	498 *415*	0.59 *0.29*	40 *67*	0.78 *0.31*	2.016 *2.053*	0.172 *0.208*
$SnNb_2O_6$	948 *940*	217 *230*	0.72 *0.64*	33 *41*	0.83 *0.34*	2.014 *2.012*	0.117 *0.160*
$BiNbO_4$	962 (954) *863 (853)*	182 (201) *180 (193)*	0.19 (0.38) *0.21 (0.65)*	21 (31) *41 (56)*	0.57 (0.31) *0.79 (0.51)*	1.998 *2.038*	0.127 *0.123*
La_3NbO_7	801 (825) *878 (875)*	139 (101) *294 (252)*	0.86 (0.85) *0.16 (0.37)*	12 (17) *43 (60)*	0.86 (0.84) *0.39 (0.21)*	1.999 *2.011*	0.015 *0.014*
$Mg_4Nb_2O_9$	869 (969) *814 (786)*	384 (393) *377 (386)*	0	43 (62) *42 (61)*	0	2.005 *2.022*	0.114 *0.116*
$CsBiNb_2O_7$	950 887	578 *584*	0.10 *0.06*	24 *17*	0.72 *0.47*	2.029 2.031	0.198 *0.164*
$Cd_2Nb_2O_7$ (t)	910 *833*	29 *91*	0.30 *0.16*	27 *19*	0.27 *0.45*	1.958 *1.974*	0.048 *0.089*
$Cd_2Nb_2O_7$ (c)	887 *791*	76 *22*	0	44 *14*	0	1.967 *1.896*	0.000 *0.000*
$Sn_2Nb_2O_7$	1108 (1146) *855*	2923 (2357) *296*	0	93 (82) *32*	0	2.101 *2.007*	0.000 *0.000*

Nb-O bond distances. Averaged and standard deviations of X-ray and optimized structures are sketched in Figure 1. Further structural details are given in the Supporting Information section (Table S1). Four coordinated Nb atoms show shorter Nb-O distances than six-coordinated Nb atoms. Except for $Sn_2Nb_2O_7$ and the cubic structure of $Cd_2Nb_2O_7$, the difference between optimized and X-ray averaged Nb-O distances is smaller than 0.05 Å. It is noteworthy to mention that most of the optimized distances are larger than X-ray ones, that is consistent with the overestimation generally observed for DFT-PBE optimized crystal structures. The discrepancy with the pyrochlores may arise from the non-stoichiometric character of these compounds, whereas stoichiometric $A_2Nb_2O_7$ (A = Cd, Sn) formula have been considered for computations. Moreover, in the case of the cubic structure of $Cd_2Nb_2O_7$, the difference between X-ray and DFT

may come from the fact that this compound undergoes a transition to a lower symmetry than the room-temperature cubic structure.

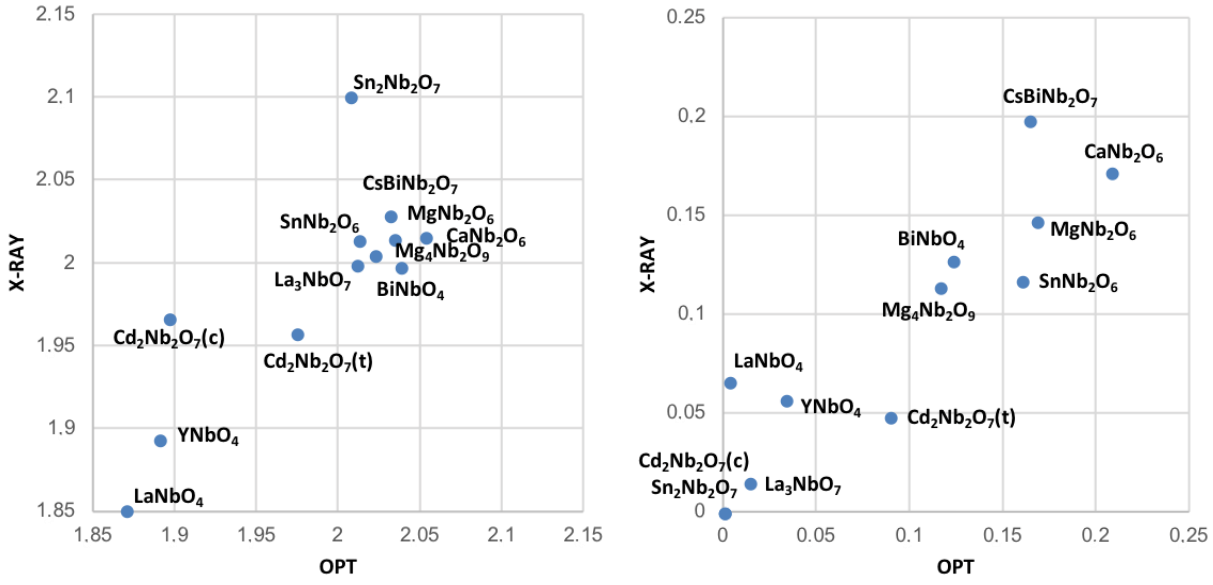

(a) ***(b)***

Figure 1. X-ray and optimized Nb-O distances of twelve structures: averaged (a) and standard deviation (b).

Quadrupolar parameters. ^{93}Nb quadrupolar coupling constant and asymmetry parameters computed for X-ray and optimized structures using the CASTEP code are sketched in Figure 2. C_Q of relaxed structures is computed lower than the one computed considering X-ray structures for $LaNbO_4$, $Sn_2Nb_2O_7$ and $Cd_2Nb_2O_7$ (t) whereas it is computed higher for $CaNb_2O_6$, $BiNbO_4$ and La_3NbO_7. The values computed for the six remaining structures are almost identical whatever the way (diffraction or *in silico* studies) they were obtained. It is noteworthy to mention that the underestimation of C_Q for $LaNbO_4$, $Sn_2Nb_2O_7$ and $Cd_2Nb_2O_7$ (t) can be linked to large differences in Nb-O distances. In $LaNbO_4$ and the tetragonal structures of $Cd_2Nb_2O_7$, Nb-O standard deviations are largely different in X-ray and optimized structures; optimized Nb-O distance in $Sn_2Nb_2O_7$ is much shorter than the X-ray one. For $CaNb_2O_6$, $BiNbO_4$ and La_3NbO_7, lengthening of Nb-O distances upon optimization goes along with an overestimation of C_Q. Larger deviations are generally computed for the asymmetry parameter compared to the quadrupolar coupling constant, since the former is obtained from the three eigenvalues of the EFG tensor whereas the latter only depends on the largest eigenvalue of this tensor. The largest deviations between X-ray and relaxed structures computed for η_Q occur for La_3NbO_7, $SnNb_2O_6$, and $CaNb_2O_6$. For the other

compounds, the difference is lower than 0.2. It is important to mention that ^{93}Nb quadrupolar parameters computed using WIEN2k are in a fairly good agreement with the one computed with the PAW approach embedded in the CASTEP code (see Table 1).

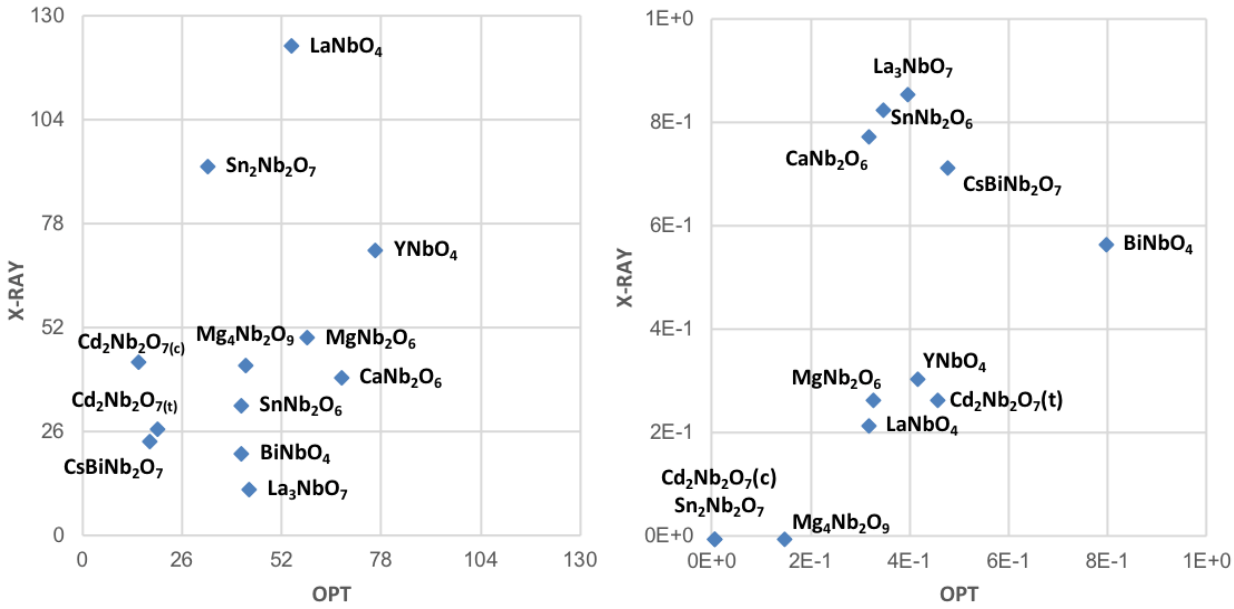

(a) ***(b)***

Figure 2. ^{93}Nb quadrupolar interaction parameters computed for X-ray and optimized structures of twelve structures: quadrupolar coupling constant, C_Q, in MHz (a) and asymmetry parameter, η_Q (b).

Chemical shift parameters. ^{93}Nb chemical shift parameters (δ_{iso}, σ_{aniso}, η_σ) computed using the GIPAW approach for X-ray and optimized structures are sketched in Figure 3. Except for La_3NbO_7 and $YNbO_4$, relaxing the geometry goes along with a decrease of the isotropic chemical shift. This was also observed by Papulovskiy et al. for several niobates [17]. The difference between both computed δ_{iso} can reach up to 150 ppm in the case of $Sn_2Nb_2O_7$. It is noteworthy to mention that using another approach than GIPAW to compute δ_{iso} leads to similar results (cf. Table 1). Whatever the method, the effect of structure relaxation on the calculation of the isotropic chemical shielding is very significant. Such an influence has often been described in the literature [37]. On the contrary, the computed anisotropic chemical shieldings do not much depend on the crystal structures, except for La_3NbO_7 and $LaNbO_4$. For the latter, σ_{aniso} is computed more than three times larger for the X-ray structures than for the relaxed one, whereas for La_3NbO_7 it is computed 150 ppm larger for the relaxed structure. In the case of $Sn_2Nb_2O_7$, the large difference between the computed valued certainly arises from the large difference of Nb-O bond distances

in X-ray and relaxed structures. It is interesting to mention that σ_{aniso} computed using the CASTEP and WIEN2K codes are very close. Finally, calculating the asymmetry parameter of the chemical shielding leads to similar results from a qualitative point of view (except for La_3NbO_7). But, differences between computed values can reach 0.25 or larger (for La_3NbO_7).

DISCUSSION

It is worth mentioning that all computed ^{93}Nb NMR parameters (either from X-ray and optimized structures) were plotted as a function of the Nb-O averaged distances or as a function of the standard deviations of the Nb-O distances (not shown here). However only poor correlations were observed (most of R^2 values were lower than 0.4) showing that ^{93}Nb NMR parameters cannot be rationalized on the basis of Nb-O bond distances.

Computed values have been compared to the experimental one; R^2 values are given in Table 2. The correlation of the computed and measured isotropic chemical shift is rather poor whatever the crystal structure considered (X-ray or optimized) whereas the correlation is good for σ_{aniso} and η_{σ}. For δ_{iso} and σ_{aniso}, the computed parameters better compare with experiments using X-ray crystal structure. On the contrary, optimizing the crystal structure of the niobates significantly improves the agreement between computed and measured ^{93}Nb quadrupolar coupling constant whereas it weakens the agreement between measured and computed values for the asymmetry parameter. It is interesting to note that ^{93}Nb NMR parameters computed in this work are overall, in a lower agreement with experimental results, compared to the results published by J. V. Hanna et al. [10]. However, this latter study is based on a slightly different set of niobates. In particular, alkaline perovskite systems were also considered as well as Bi_3NbO_7. Moreover, the version of the codes they used is different from the one used in this study.

TABLE 2. R^2 values of ^{93}Nb NMR parameters: experimental data *vs* computed ones (X-ray and optimized structures).

	δ_{iso}	σ_{aniso}	η_{σ}	C_Q	η_Q
X-ray *vs* exp.	0.24	0.93	0.63	0.28	0.55
Optimized *vs* exp.	0.13	0.81	0.64	0.62	0.28

CONCLUSIONS

In this study, we performed DFT calculations of ^{93}Nb parameters for twelve structures of niobates. A special attention was paid to the influence of structure relaxation on the computed spectroscopic

properties. We demonstrated that structural parameters can play a part in the calculations of both quadrupolar interaction and chemical shift parameters of ^{93}Nb in various niobates. We also showed that, from a qualitative point of view, most of the quadrupolar interaction and chemical shift parameters are computed similar whatever the DFT code used.

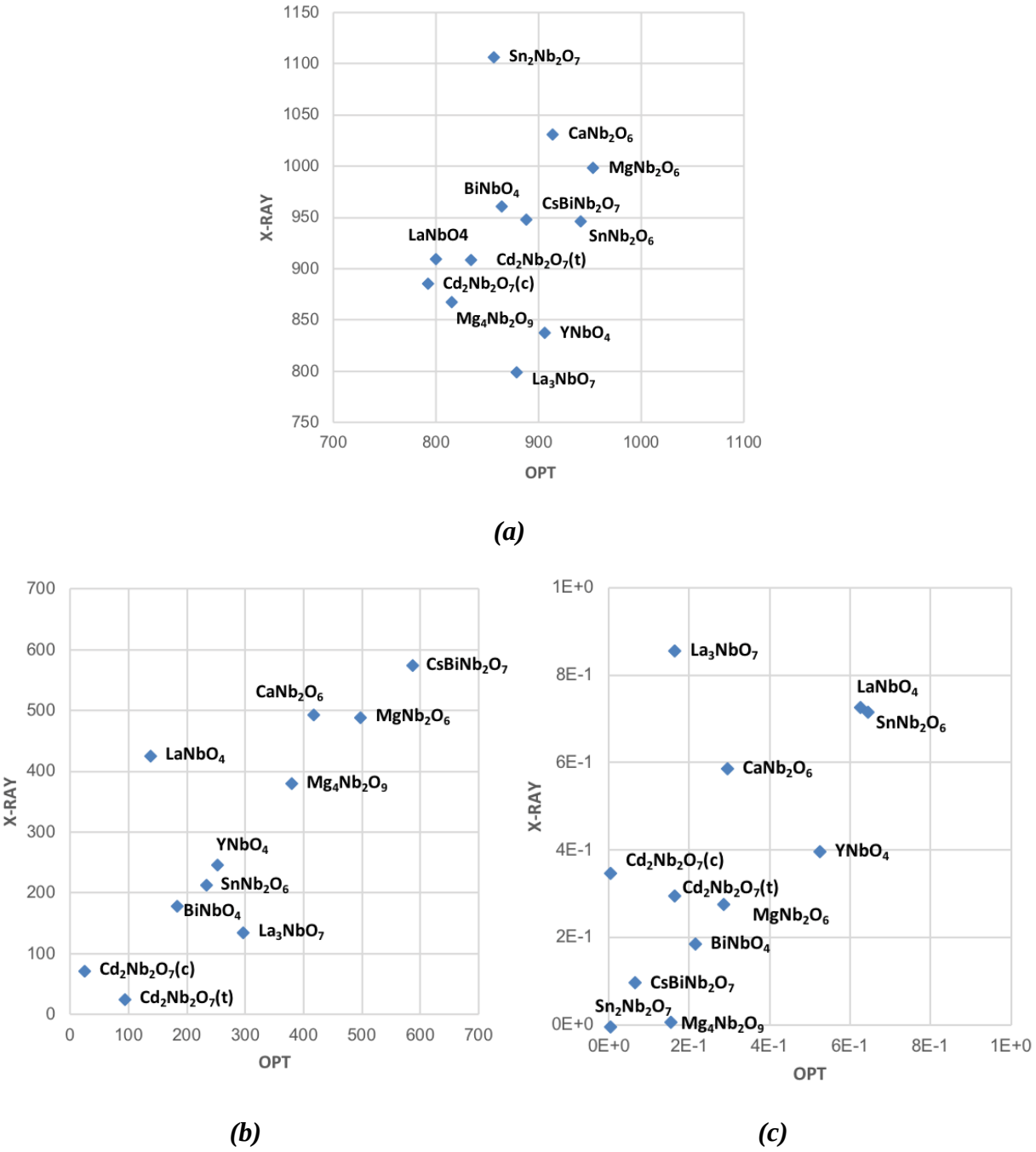

Figure 3. ^{93}Nb chemical shift parameters computed for X-ray and optimized structures of twelve structures: isotropic chemical shift, δ_{iso}, in ppm (a), anisotropic chemical shielding, σ_{aniso} in ppm (b), and asymmetry parameter, η_σ (c).

References

1 D. E. Ellis, D. Guenzburger, H. B. Jansen, *Phys. Rev. B*, **28**, 3697 (1983)

2 L. Hemmingsen, R. Bauer, M. J. Bjerrum, K. Schwarz, P. Blaha, P. Andersen, *Inorg. Chem.*, **38**, 2860 (1999)

3 M. Iglesias, K. Schwarz, P. Blaha, D. Baldomir, *Phys. Chem. Minerals*, **28**, 67 (2001)

4 S. Hafner, *J. Phys. Chem. Solids*, **27**, 1881 (1966)

5 P. R. Sarode, A. R. Chetal, *J. Phys. F: Met. Phys.*, **7**, 1103 (1977)

6 D. E. Smiles, G. Wu, P. Hrobaŕik, T. W. Hayton, *J. Am. Chem. Soc.*, **138**, 814 (2016)

7 P. Blaha, K. Schwarz, P. Herzig., *Phys. Rev. Lett*., **54**, 1192 (1985)

8 P. E. Blöchl., *Phys. Rev. B*, **50**, 17953 (1994)

9 C. J. Pickard, F. Mauri., *Phys. Rev. B*, **63**, 245101(2001)

10 T. Charpentier., *Solid State Nucl. Magn. Reson.*, **40**, 1(2011)

11 C. Bonhomme, C. Gervais, N. Folliet, F. Pourpoint, C. Coelho Diogo, J. Lao, E. Jallot, J. Lacroix, J-M. Nedelec, D. Iuga, J. V. Hanna, M. E. Smith, Y. Xiang, J. Du, D. Laurencin., *J. Am. Chem. Soc.*, **134**, 12 (2012)

12 C. Bonhomme, C. Gervais, F. Babonneau, C. Coelho, F. Pourpoint, T. Azaï, S. E. Ashbrook, J. M. Griffin, J. R. Yates, F. Mauri, C. J. Pickard, *Chem. Rev.*, **112**, 5733 (2012)

13 R. Laskowski, P. Blaha, *Phys. Rev. B*, **85** , 035132 (2012)

14 R. Laskowski, P. Blaha, P. *Phys. Rev. B*, **89**, 014402 (2014)

15 B. Zhou, V. K. Michaelis, Y. Yao, B. L. Sherriff, S. Kroeker, Y. Pan, *CrystEngComm*, **16**, 10418 (2014)

16 J. V. Hanna, K. J. Pike, T. Charpentier, T. F. Kemp, M. E. Smith, B. E. G. Lucier, R. W. Schurko, L. S. Cahill, *Chem. Eur. J.*, **16**, 3222 (2010).

17 E. Papulovskiy, A. A. Shubin, V. V. Tersikh, C. J. Pickard, O. B. Lapina, *Phys. Chem. Chem. Phys.*, **15**, 5155 (2013)

18 J. Cuny, E. Furet, R. Gautier, L. Le Pollès, C. J. Pickard, J.-B. d'Espinose de Lacaillerie, *ChemPhysChem*, **10**, 3320 (2009)

19 J. Cuny, K. Sykina, B. Fontaine, L. Le Pollès, C. J. Pickard, R. Gautier, *Phys. Chem. Chem. Phys.* **13**, 2245 (2011)

20 R. S. Roth., J. L. Waring, *Am. Mineral*., **48**, 1348 (1963)

21 D. Michel, L. Mazerolles, M. Perez,Y. Jorba., *J. Mater. Sci.*, **18**, 2618 (1983).

22 S. Pagola, R. E. Carbonio, J. A. Alonso, M. T. Fernández-Día., *J. Solid State Chem.*, **134**, 76 (1997)

23 J. P. Cummings, S. H. Simonsen., *Amer. Miner.*, **55**, 90 (1970)

24 P. Cerny, A.-M. Fransolet, T. S. Ercit, R. Chapman, *Can. Mineral*., **26**, 889 (1988)

25 B. Muktha, J. Darriet , G.Madras, T. N. Guru Row, *J. Solid State Chem.*, **179**, 3919 (2006)

26 H. J. Rossell, *J. Solid State. Chem*., **27**, 115 (1979)

27 N. Kumada, K. Taki, N. Kinomura., *Mater. Res. Bull*., **35**, 1017 (2000)

28 J. Zhang, X. Wang, D. Wu, L. Liu, H. Zhao, *Chem.Mater*., **21**, 1296 (2009)

29 K. Lukaszewicz, A. Pietraszko, J. Stepien-Damm, *Mater. Res. Bull*., **29**, 987(1994)

30 M. T. Weller, R. W. Hughes, J. Rooke, C. S. Knee, J. Reading, *Dalton Trans.*, **19**, 3032 (2004)

31 L. P. Cruz, J.-M. Savariault, J. Rocha, *Acta Cryst.* **C57**, 1001 (2001)

32 M. D. Segall, P. J. D. Lindan, M. J. Probert, C. J. Pickard, P. J. Hasnip, S. J. Clark, M. C. Payne, *J. Phys.: Condens. Matter* **14**, 2717 (2002)

33 J. P. Perdew, K. Burke, M. Ernzerhof., *Phys. Rev. Lett*., **77**, 3865 (1996)

34 H. J. Monkhorst, J. D. Pack, *Phys. Rev. B* , **13**, 5188 (1976)

35 K. Schwarz, P. Blaha, G. K. H. Madsen, *Comput. Phys. Commun*., **147**, 71 (2002)

36 K. Schwarz, P. Blaha, *J. Comput. Mater. Sci.*, **28**, 259 (2003)

37 J. Cuny, R. Gautier, J.-F. Halet, in *Handbook of Solid-State Chemistry*, eds. R. Dronskowski, S. Kikkawa & A. Stein, Wiley-VCH (2017), 16, 607-646